THREE-DIMENSIONAL NUMERICAL SIMULATION OF SEDIMENT CONTROL AT LATERAL DIVERSION

OTA KAZUYUKI

Central Research Institute of Electric Power Industry, Chiba, Japan, k-ota@criepi.denken.or.jp

SATO TAKAHIRO

Central Research Institute of Electric Power Industry, Chiba, Japan, t-sato@criepi.denken.or.jp

ABSTRACT

Submerged vane is used in preventing excessive bed-sediment ingestion into lateral diversions of flow from alluvial channels. This study presents three-dimensional sediment transport simulation at lateral diversion with or without submerged vane. The hybrid RANS-LES approach is used in hydrodynamic model to reasonably resolve coherent turbulence structure around the diversion entrance. The Lagrangian approach is used to compute the nonequilibrium bed load transport. Simulation showed that submerged vanes decrease in bed load ingestion into the diversion. Influence of the coherent turbulence structure is revealed by simulation. The result also implies that the present numerical simulation becomes a power tool to examine the vane effect.

1. INTRODUCTION

During the past several decades, submerged vanes have been extensively used for reducing the movement of bed sediment into diversions, especially riverside water intakes for hydropower and municipal water supply utilities. The design guideline of the vane work has been established through several fundamental studies or field installation (Odgaard, 2009). Since the diversion with vane produces complicated flow pattern of water and sediment, the effect of the vane has been examined by the flume experiment or scaling physical modeling. Barkdoll et al. (1999) quantified the vane effect by movable-bed experiments. They reported that sediment transport into the diversion is successfully interrupted by the vane if the flow contraction is weak at the diversion. However, when the flow contraction is strong at the diversion, the intermittent turbulence entrains bed sediment around a vane and diminishes the vane effect. Due to limitation of experimental technique, there are still unknowns on the flow structure around the vane and its influence on the vane effect.

Recently, three-dimensional sediment transport simulation made a great progress. The numerical simulation technology allows for revealing relationship between three-dimensional flow and sediment transport around hydraulic structures. Koken and Constantinescu (2008) have applied LES (Large Eddy Simulation) to resolve 3D turbulence flow around a vertical-wall spur dike on the rigid flat bed and the rigid scoured bed. They demonstrated that coherent flow structures play important roles on morphological change around a hydraulic structure and that formation of the coherent flow depends on the bed condition. However, their simulation lacks sediment transport module and thus temporal variation of the coherent structure and bed topography is not presented. Nagata et al. (2005) coupled RANS equation and bed load model based on the Lagrangian approach. They simulated local scour around a vertical-wall spur dyke with sufficient accuracy. Ota et al. (2017a) coupled the Lagrangian approach by Nagata et al. (2005) and LES to simulate sediment transport around permeable spur dyke considering intermittent turbulent structure. They simulated the movable-bed experiment with sufficient accuracy. However, the LES requires small cell size for all computational cell enough to resolve the turbulence. More reasonable approach is required if the large domain is simulated.

This study attempts three-dimensional sediment transport simulation of lateral diversion with or without submerged vane to study complicated flow pattern of water and sediment at diversion. The hybrid RANS-LES approach is used in hydro dynamic model to reasonably resolve turbulence structure around the diversion entrance. The Lagrangian approach is used to compute the nonequilibrium bed load transport. The vane effect is examined by simulation result. Influence of the coherent structure at the vane is also discussed.

2. NUMERICAL MODEL

2.1 Hydrodynamic model

The hydrodynamic model consists of Navier–Stokes equation for the incompressible air-water flow that considers seepage flow and profile evolution in a sediment. The model assumes sufficiently small temporal variation in the porosity λ representing the volume fraction of void space in each cell. The porosity becomes $\lambda = 1$ for pure fluids, $0 < \lambda < \eta$ for water-sediment interface, and $\lambda = \lambda_b$ for pure sediment region where η is the porosity of the sediment itself. The governing equations for continuity and momentum of fluid are given as follows:

$$\frac{\partial}{\partial x_j}\left(\lambda \rho u_j\right) = 0 \tag{1}$$

$$\lambda \frac{\partial}{\partial t}\left(\rho u_i\right) + \frac{\partial}{\partial x_j}\left(\lambda \rho u_i u_j\right) = -\lambda \frac{\partial p}{\partial x_i} + \frac{\partial}{\partial x_j}\left[\left(\mu + \mu_t\right)\frac{\partial u_i}{\partial x_j}\right] + \lambda \rho g_i + A u_i \tag{2}$$

where u_j = velocity; ρ = fluid density, p = pressure; g_i = the gravitational acceleration vector; v = kinetic viscosity; v_t = turbulent kinetic viscosity; A = drag coefficient of porous media which assumes the Darcy's law. VOF (Volume of Fluid) method is used for capturing the water surface. To solve the velocity-pressure coupling, the pressure implicit with splitting of operator (PISO) approach was adopted. The Scale Adapted version of $k-\varpi$ SST (SST-SAS) model by Menter and Egorov (2005) is used to compute the effect of turbulence. The SST-SAS is one of the hybrid RANS-LES models which allow for resolving turbulent fluctuation in a reasonable computational cost. The equations of k and ϖ become as follows.

$$\frac{\partial k}{\partial t} + \frac{\partial}{\partial x_j}\left(u_j k\right) - \frac{\partial}{\partial x_j}\left[\left(v + \sigma_k v_t\right)\frac{\partial k}{\partial x_j}\right] = P_k - \beta^* \omega k \tag{3}$$

$$\frac{\partial \omega}{\partial t} + \frac{\partial}{\partial x_j}\left(u_j \omega\right) - \frac{\partial}{\partial x_j}\left[\left(v + \sigma_\omega v_t\right)\frac{\partial \omega}{\partial x_j}\right] = \frac{\gamma}{v_t}G - \beta \omega^2 + 2\left(1 - F_1\right)\frac{\sigma_{\omega 2}}{\omega}\frac{\partial k}{\partial x_j}\frac{\partial \omega}{\partial x_j} + P_{SAS} \tag{4}$$

$$\text{with } F_1 = \tanh\left(\text{arg}_1{}^4\right) \text{ and } \text{arg}_1 = \min\left(\max\left(\frac{\sqrt{k}}{\beta^* \omega y}; \frac{500v}{y^2 \omega}\right); \frac{4\rho \sigma_{\omega 2} k}{CD_{k\omega} y^2}\right) \tag{5}$$

$$F_2 = \tanh\left(\text{arg}_2{}^4\right) \text{ and } \text{arg}_2 = \max\left(2\frac{\sqrt{k}}{\beta^* \omega y}; \frac{500v}{y^2 \omega}\right) \tag{6}$$

$$P_k = \min\left(\frac{\partial u_i}{\partial x_j}\left(\frac{\partial u_i}{\partial x_j} + \frac{\partial u_j}{\partial x_i}\right), 10\beta^* k\omega\right) \tag{7}$$

$$v_t = \frac{a_1 k}{\max\left(a_1 \omega, S F_2\right)} \tag{8}$$

$$P_{SAS} = F_{SAS}\max\left(\zeta_2 \kappa S^2 \sqrt{\frac{L}{L_{vk}}} - \frac{2}{\alpha k}\max\left(\frac{1}{\omega^2}\frac{\partial \omega}{\partial x_j}\frac{\partial \omega}{\partial x_j}, \frac{1}{k^2}\frac{\partial k}{\partial x_j}\frac{\partial k}{\partial x_j}\right), 0\right) \tag{9}$$

where β^*, σ_k, σ_ω, $\sigma_{\omega 2}$, σ_t, a_1, and F_{SAS} are constants that are used in Menter and Egorov (2005). Note that a higher ω due to the P_{SAS} term reduces k, subsequently reducing the modeled turbulent viscosity and its damping effect on the resolved flow. This allows generation of resolved turbulent fluctuations in the velocity field. Although the momentum equation treats seepage flow, the turbulence model acts only effectively above the bed. In other words, the water-sediment interface is dealt by the wall function in the turbulence model.

The hydrodynamic model uses the open-sourced CFD library OpenFOAM. The equations are discretized using FVM method. TVD scheme is used in the convection terms of equations of momentum and turbulence. MUSCL scheme is used in the VOF computation. Implicit Euler method is used for temporal development. Time step is dynamically decided so that the CFL condition is satisfied.

2.2 Sediment transport model

The sediment transport model uses a Lagrangian method by Nagata et al. (2005) to simulate the non-equilibrium bed load transport. The computation starts from sediment pick-up at a stationary bed in each computational cell on the bed surface. The bed load particles picked up from the bed are tracked using the Lagrangian method with the motion equation for a bed load particle. The bed surface deforms as a result of sediment exchange between the bed load and the stationary bed (i.e., the pick-up and the deposition).

The volume of sediment pickup per unit time from a computational cell on the bed surface, V_p, is given by:

$$V_p = (1 - \lambda_b) d p_s S_b \tag{10}$$

where p_s is the pickup rate, d is the diameter of the sediment particle, λ_b is the bed porosity, and S_b is the area of the bed-surface mesh. The pickup rate p_s is obtained from the equation established by Nakagawa et al. (1986), which includes the effect of the local bed slope on sediment motion:

$$p_s \sqrt{\frac{d}{(\sigma/\rho - 1)g}} = 0.03 G_* \tau_* \left(1 - 0.7\phi \frac{\tau_{*c}}{\tau_*}\right)^{m_p} \tag{11}$$

where τ_* and τ_{*c} are bed shear stress and critical bed shear stress, respectively; G_* = a coefficient accounting for the directional deviation between the near-bed velocity and sediment movement; ϕ = function accounting for the effect of bed slope.

Location of the bed load particle is computed for each particle class as follows:

$$p_{sed,j} = \int u_{sed,j} \, dt \, , \quad s_{sed} = \int |u_{sed}| \, dt \tag{12}$$

where j (=1, 2) represents the tangential direction to the local bed surface. p_{sed} = location of the bed load particle, s_{sed} = total moved distance of bed load particle after pick-up, u_{sed} = velocity of bed load particle computed by motion equation considering fluid drag, submerged particle weight, bed friction, and added mass as follows:

$$\rho \left(\frac{\rho_s}{\rho} + C_M\right) \frac{\pi d^3}{6} \frac{\partial u_{sed,j}}{\partial t} = Dr_j + W_j - F_j \tag{13}$$

where Dr, W, and F represent fluid drag, submerged particle weight, and bed friction. Please see Ota et al. (2017b) for detail of each term.

Although the Lagrangian model tracks a parcel of bed load particles, in reality all bed load particles included in a parcel does not always behave in the same manner. For example, some of particles in a parcel continue moving, whereas others may be deposited on the bed surface. Since these phenomena are related to fluid turbulence or irregularity of the bed roughness, the stochastic approach is connected to the Lagrangian method. The sediment volume of deposition V_d along the bed load transport trajectory are computed using the probability density function:

$$V_d^{(n)} = V_p f_s \left(s_{sed}^{(n)}\right) \Delta s_{sed} \tag{14}$$

$$\text{with} \quad f_s \left(s_{sed}^{(n)}\right) = \frac{1}{\Lambda} \exp\left(-\frac{s_{sed}^{(n)}}{\Lambda}\right) \tag{15}$$

where superscript (n) represents the nth step after a sediment pick-up; $f_s (s_{sed}^{(n)})$ = the probability density function of the step length; Λ = the average step length, which is calculated by the following equation (Armanini, 2015).

$$\frac{\Lambda}{d} = \frac{K_1}{1 + K_2/\tau_*} \tag{16}$$

where K_1 and K_2 are constant ($K_1 = 150$, $K_2 = 1$).

Using the volumes of sediment pickup and sediment deposition, which are calculated as previously described, the temporal variation in bed elevation is expressed as follows:

$$(1 - \lambda_b) \frac{\partial z_b}{\partial t} = \frac{\sum_{n=1}^{N} V_d^{(n)} - V_p}{S_d} \tag{17}$$

where z_b is the bed elevation, and S_d is the projected area of the computational cell in which the sediment is deposited. The summation of $V_d^{(n)}$ represents the total volume of deposited sediments in each computational cell at each time step

When local scour occurs because of the presence of a hydraulic structure, the local bed slope in the scour hole becomes steep. When the local bed slope θ_b exceeds a critical value θ_{bc}, sliding of bed materials occurs around the structure. Thus, assuming that the sliding event takes place instantly, the sliding sediment volume required to keep the bed slope at its critical value θ_{bc} is calculated when θ_b exceeds the critical value θ_{bc}, which is assumed to be the angle of repose in water. The volume of sliding sediment is then added to the pickup volume at the mesh region where the sliding event takes place.

In the present scheme, the position at which the deposition volumes were obtained did not necessarily coincide with the numerical grid points. Therefore, the mesh region with the location of the moving sediment particle was found at each time step, and the deposition volume was distributed proportionally to each grid point based on the relative location of the particle.

3. RESULT AND DISCUSSION

3.1 Simulation case

Barkdoll et al. (1999) conducted laboratory experiments using a flume fitted with a $90°$, lateral-diversion channel, as depicted in Fig. 3. The flume channel was 24 m long and 1.5 m wide. The diversion channel was 2.44 m long and 0.61 m wide. The diversion floor elevation was level with the initial bed level in the flume. The experiments were conducted under the rigid-bed condition and the movable-bed condition. The rigid-bed experiment was conducted to measure flow velocity at near bed in the lateral channel without vane. The movable-bed experiment was conducted to examine the effect of vanes by setting uniform sediment with d = 0.9 mm instead of rigid-bed. No sediment was supplied from the upstream end. The rigid-bed and movable-bed experiment are simulated in the present study. Hydraulic conditions for all simulation of this study is as follows: Flume flow rate is 0.104 m^3/s and initial water depth is 0.152 m upstream of the diversion. For this flow condition, the flume's sand bed was in a dune regime, with sand moved as bed load. Flow rate at lateral channel is 0.01 m^3/s equivalent to 10 % of upstream flume flow rate. To quantify influence of diversion rate Barkdoll et al. (1999) used the ratio q_r (unit discharge in the diversion) / (unit discharge in the flume). The condition of q_r = 0.25 is simulated in the present study.

The present study conducted two numerical simulations of movable-bed experiment with and without vane. Figure 1 shows the region of simulation run with vanes. A three-row array of vanes was allocated in front of the inlet of lateral diversion. Computational cell size was set to be 1 ~ 3 cm depending on location. 1.5 million computational cells were totally used in simulation. The vane was created as impermeable face of the computational cell (see Figure 1(a)).

As to boundary conditions, flow rate was fixed in the inlet boundary and the outlet boundary of the lateral channel. Flow depth was adjusted in the outlet of the main flume. These inlet and outlet boundary condition were consistent with that in the experiment. Non-slip condition was imposed on the wall boundary. There was no boundary condition on the bed surface because the porous medium was assumed to be the bed. Sand roughness was considered in the turbulence model.
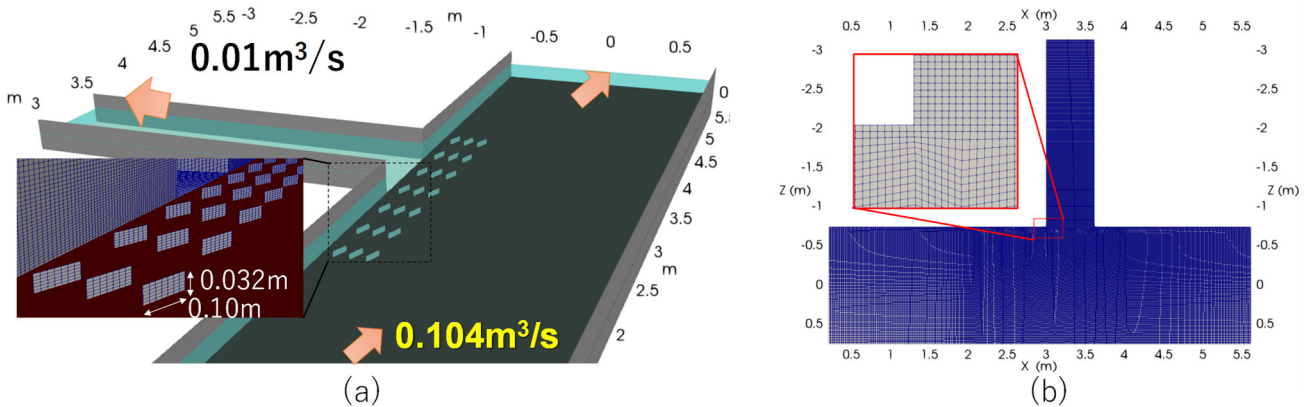

Figure 1. (a) Bird's eye view of computational domain of run with vanes, (b) horizontal plane of computational cell

3.2 Simulation result

3.2.1 Rigid-bed condition

In the rigid-bed experiment, the flow pattern is shown by the velocity measurement at 2 mm above the bed. Figure 2 shows the near-bed stream line of the experiment and simulation. There is no vane at the intake of the lateral channel. The simulation in Figure 2(b) also shows the magnitude of flow velocity using color. There is detached flow at the left-bank side of the lateral channel in both experiment and simulation. Size and shape of the detached flow are similar between experiment and simulation, which has two centers of vortex. The size of the vortex in the detached flow is different between experiment and simulation due to difficulty of resolution of the vortex in the vicinity of the bed. However, what is importance for evaluation of sediment ingestion is accuracy of the detached flow and flow contraction at the diversion entrance. The simulation result represents the detached flow and flow contraction around the diversion entrance very well. This context assures the

correctness of the hydro dynamic model for achieving the objective of this study. It is worth noting that the authors also used the standard $k - \varpi$ SST model as a preliminary work. The SST-SAS model showed better accuracy compared to the standard $k - \varpi$ SST model.
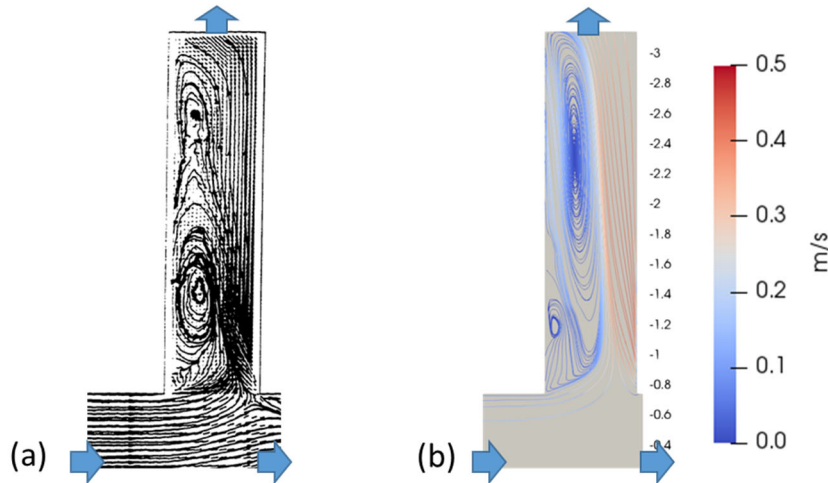

Figure 2. Stream line of near-bed flow velocity on the lateral channel in (a) experiment and (b) simulation

3.2.2 Movable-bed condition

Figures 3 shows bed shapes in simulation run without vane. Sand dunes are observed in the main flume. Bed load on the sand dune is clearly ingested into the lateral channel. Sediment in the lateral channel deposits mainly left-bank side because of the low flow velocity in the recirculating region (see Figure 2). Figure 3 also shows scour holes along flume wall of the main channel around the diversion entrance, as one reported in Barkdoll et al. (1999). Figure 4 shows bed shapes in simulation run with vane. The vanes clearly cause local scour hole and deposition around themselves, which is closely related to the effect of vane on sediment control. Sediment scoured by the vanes deposits again at the right-bank side of the scoured region, because the direction of bed load motion is affected by the vanes. There also exists sediment deposition in the left-bank side of lateral channel, as is seen in simulation run without vane. However, their volume and pattern are different from run without vane. While run without vane has much deposition region near the diversion entrance, run with vane has little deposition region there. This difference comes from the route of bed load moving to the lateral channel. In run with vane, local scour hole around the diversion entrance prevents ingestion of bed load into the lateral channel to some extent. Thus, the route of bed load into the lateral channel is limited in run with vane.

Figure 5 shows comparison of runs with and without vane regarding deposition volume in the lateral channel. Run with vane has less deposition volume in most times, which highlight the effect of the vane. It is worth noting that deposition volume is comparable at 3 ~ 4 h. This result means that the effect of vane can be temporarily weak, because the vane effect is affected by the bed shape. This mechanism is also closely related to the turbulent structure around vanes, as mentioned later.

Figure 6 shows the stream line of the near-bed flow at 2 h and 4 h in runs with and without vane. The seed of stream line is allocated at 1.5cm for (a)~(d) and 4.0 cm for (e)~(f) above the initial bed elevation in the upstream region, following to temporal bed aggradation. Figures 6(a)(c) depict near-bed flow going to the diversion entrance without vane, which implies that the near-bed flow forces bed load to move into the diversion entrance. Figure 6(a) also depicts the scour hole and secondary vortex around the downstream corner of the diversion entrance, as one reported in Barkdoll et al. (1999). Figures 6(b)(d) depict more complicate flow pattern around the vane. By the vanes the near-bed flow is forced to direct the opposite bank side of the diversion entrance. This flow pattern appears especially in earlier time as shown in Figures 6(b). More flow ingestion to the diversion entrance is seen in later times (Figures 6(d)(f)). It is worth noting that Figures 6(d) shows the very complicated flow pattern around the vane entrance, which is related to decrease in the vane effect in 3 ~ 4 h (see Figure 5). Barkdoll et al. (1999) reported that the wake vortices shed from several vanes forced bed sediment into diversion under the condition of $q_r > 0.2$. Such wake vortices are also included in Figure 6(d). Figure 7 shows the detailed flow structure around the diversion entrance in 4 h which corresponds to Figures 6(d). The isosurface is drawn by Q criterion (Dubief and Delcayre, 2000) that is the second invariant of the velocity gradient tensor and represents the vortex envelope. We see the coherent flow structure around the vane. The horseshoe vortex and wake occur at the vane adjacent to the diversion entrance. The wake goes to the diversion, as Barkdoll et al. (1999) indicated. The flow ingestion due to wake is major

mechanism of diminishing the vane effect on sediment control when $q_r > 0.2$. Since the coherent structure is unsteady phenomenon and affected by the bed shape, the effect of vane also varies in time as shown in Figure 5. If the horseshoe vortex and wake entrain more bed sediment, it leads to decrease the vane effect. To enhance the vane effect, additional measure is needed to reduce the flow velocity around the vane entrance, as indicated in Barkdoll et al. (1999). Besides, we see Figures 6(d)(f) that several vanes are buried. Several buried vanes diminish the sediment control function of the whole vanes. This is another limitation of the submerged vane work, which may require the dredge.

As long as the authors know, this is the first study to examine the vane effect of sediment control using three-dimensional sediment transport simulation considering. The simulation result showed that the vane effect is strongly affected by the turbulence coherent structure and bed shape. Such properties are not usually quantified by the conventional laboratory experiment due to limitations of measurement technique. The present numerical simulation has potential to overcome such experimental difficulty and become a power tool to understand the unsteady vane effect.
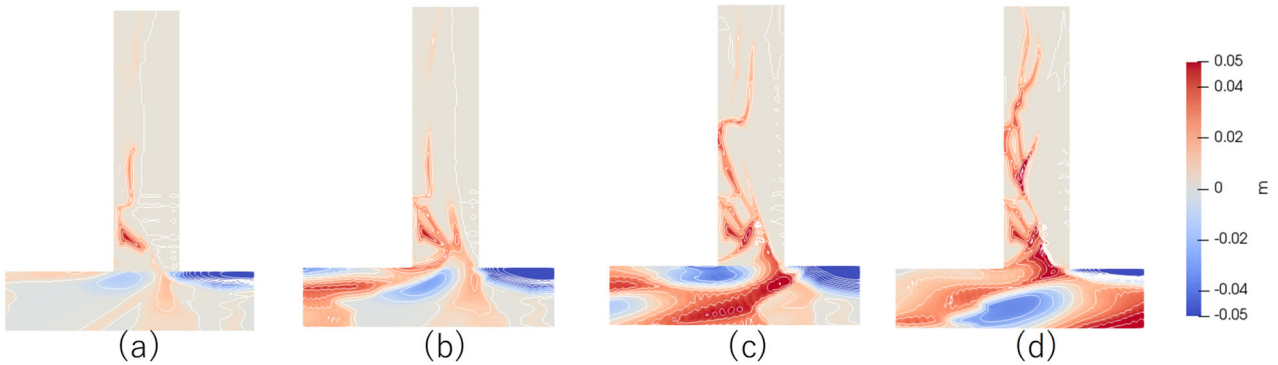
Figure 3. Temporal variation bed shape in simulation run with vane in (a) 2 h, (b) 4 h, (c) 6 h, and (d) 8 h
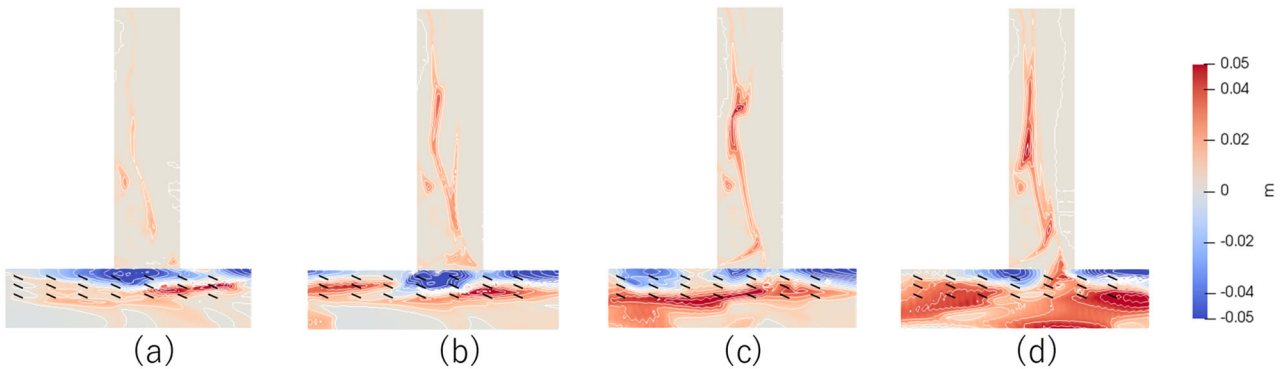

Figure 4. Temporal variation bed shape in simulation run without vane in (a) 2 h, (b) 4 h, (c) 6 h, and (d) 8 h
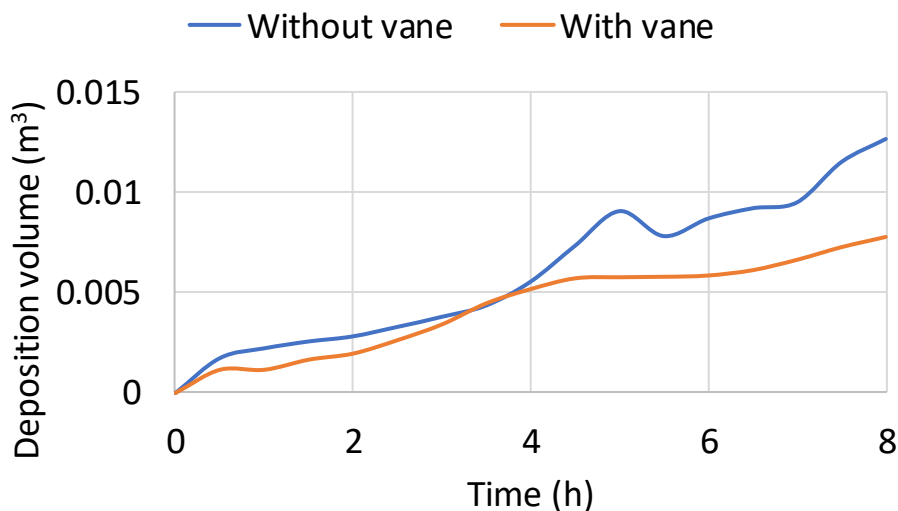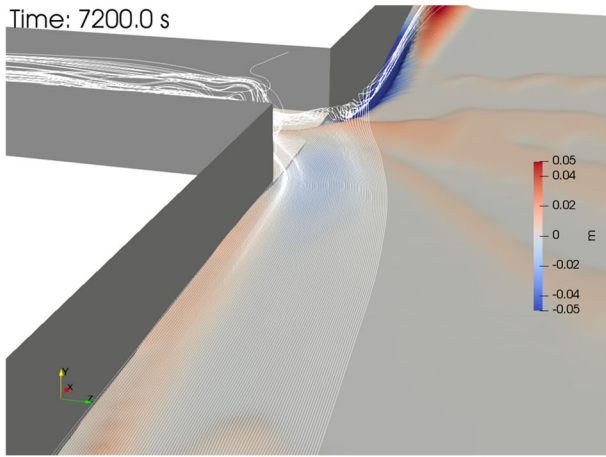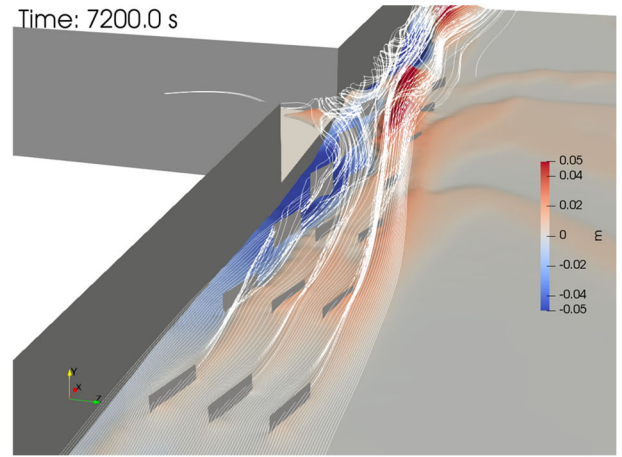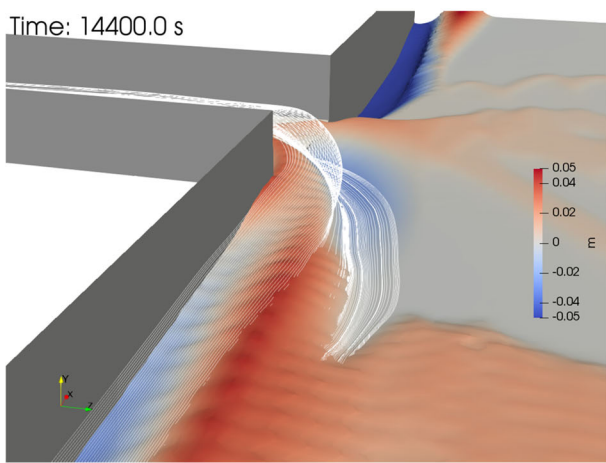

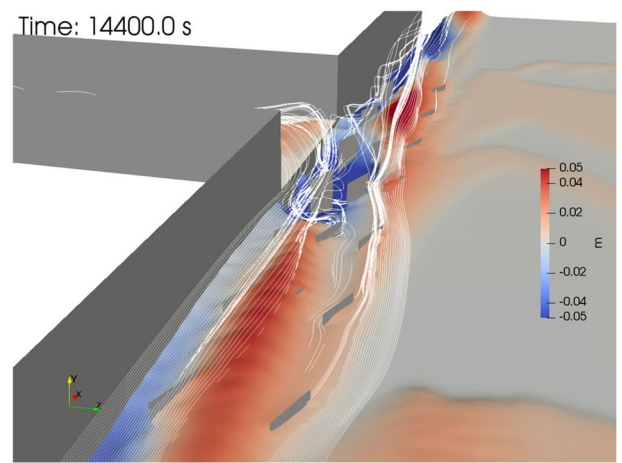Figure 5. Temporal variation of deposition volume in the lateral channel
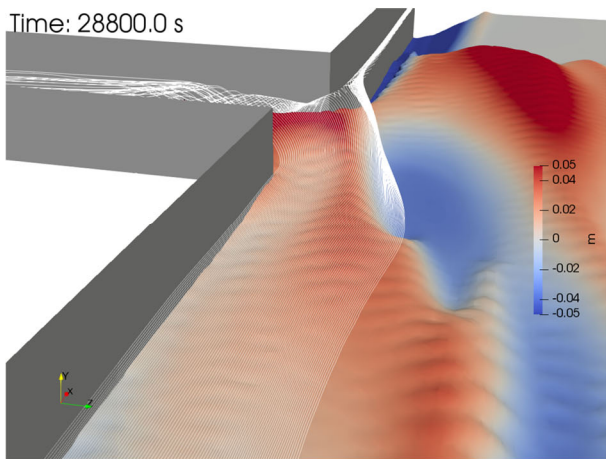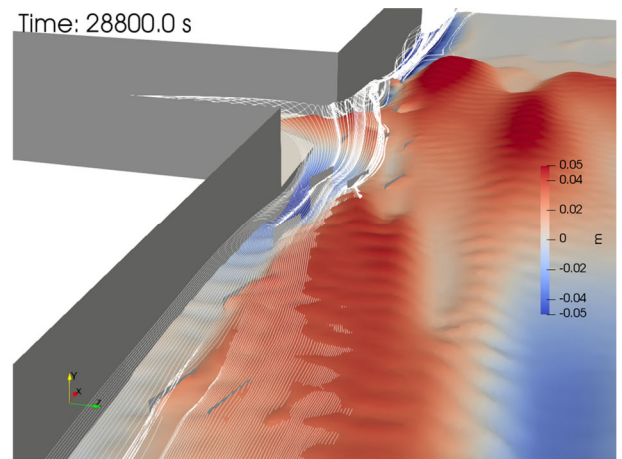
Figure 6. Stream line of near-bed flow: (a) w/o vane in 2 h, (b) w/ vane in 2 h, (c) w/o vane in 4 h, (d) w vane in 4 h, (e) w/o vane in 8 h, (f) w vane in 8 h: The seed of stream line is 1.5cm for (a)~(d) and 4.0 cm for (e)~(f) above the initial bed elevation in the upstream region.
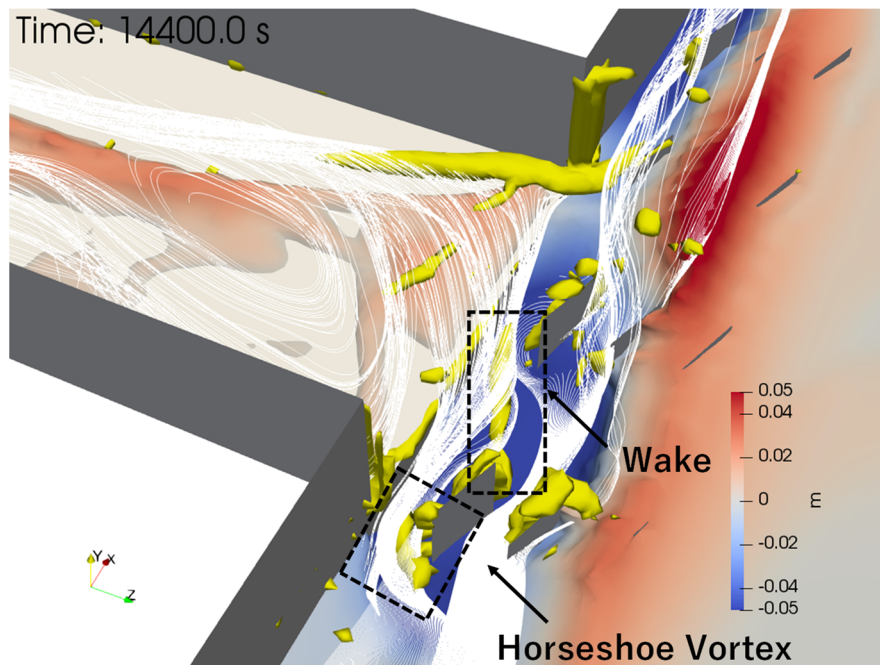
Figure 7. The coherent flow structure around the vane visualized with stream line and Q-criteria in 4 h: The horseshoe vortex and wake are enclosed by broken line.

4. CONCLUSIONS

This study presented three-dimensional simulation of sediment transport to examine the effect of submerged vane for sediment control of lateral diversion. The hybrid RANS-LES approach is used in hydrodynamic model to resolve turbulence structure around the diversion entrance. The Lagrangian approach was used to compute the nonequilibrium bed load transport. The flow velocity filed in rigid-bed experiment was simulated in a sufficient accuracy. The feature of bed shape in movable-bed experiment was also captured by the simulation. Simulation without vane showed clear bed load ingestion into the diversion, which is caused by the flow acceleration in the diversion. Simulation with vane resulted in decrease in bed load ingestion into the diversion. It is notable that the vane effect of sediment control varies in time owing to the influence of bed shape and flow structure. The horseshow vortex and wake around a vane play a roll of conveying bed sediment into the diversion, leading to diminish the vane effect of sediment control.

As long as the authors know, this is the first study to examine the vane effect of sediment control using three-dimensional sediment transport simulation. The result implies that the present numerical simulation becomes a power fool to examine the vane effect for practical objective.

REFERENCES

Armanini, A., Cavedon, V., and Righetti, M. (2015). A probabilistic/deterministic approach for the prediction of the sediment transport rate. *Adv. Wat. Res.* 81:10-18.

Barkdoll, B. D., Ettema, R., and Odgaard, A. J. (1999) Sediment control at lateral diversions: limits and enhancements to vane use, *J. Hydraul. Eng.*, 125(8):862-870.

Dubief, Y., and F. Delcayre (2000), On coherent vortex identification in turbulence, *J. Turbul.*, 1, paper 11, doi:10.1088/1468-5248/1/1/011.

Koken, M., and Constantinescu, G. (2008). An investigation of the flow and scour mechanisms around isolated spur dikes in a shallow open channel: 1. Conditions corresponding to the initiation of the erosion and deposition process. *Wat. Resour. Res.*, *44*(8).

Menter F, and Egorov Y. (2005). Ascale-adaptive simulation model using two-equation models. AIAA 2005;1095.

Nagata, N., Hosoda, T., Nakato, T., and Muramoto, Y. (2005). Three dimensional numerical model for flow and bed deformation around river hydraulic structures. *J. Hydraul. Eng.*, 10.1061/(ASCE)0733-9429(2005)131:12(1074), 1074–1087.

Nakagawa, H., Tsujimoto, T., and Murakami, S. (1986). Non-equilibrium bed load transport alongside slope of an alluvial stream. *Proc. 3rd Int. Symp. River Sedimentation*, University of Mississippi, Oxford, MS, 885–893.

Odgaard, A. J. (2009). River training and sediment management with submerged vanes. *American Society of Civil Engineers.*

Ota, K., Nakagawa, H., and Zhang, H. (2017a) Eulerian-Lagrangian simulation of bed-material load transport around partially permeable and impermeable spur dykes, *Proc. 37th IAHR World Cong.*, 583-592.

Ota, K., Sato, T., and Nakagawa, H. (2017b). Quantification of spatial lag effect on sediment transport around a hydraulic structure using Eulerian–Lagrangian model. *Adv. Wat. Resour.*, 129:281-296.